GEOLOGY | THE GEOLOGICAL SOCIETY OF AMERICA®

https://doi.org/10.1130/G45446.1

Manuscript received 1 August 2018
Revised manuscript received 20 November 2018
Manuscript accepted 17 March 2019

The relation between viscosity and acoustic emissions as a laboratory analogue for volcano seismicity

James Clarke[1], Ludmila Adam[2], Joel Sarout[3], Kasper van Wijk[1], Ben Kennedy[4], and Jeremie Dautriat[3]
[1]Department of Physics, University of Auckland, Auckland 1142, New Zealand
[2]School of Environment, University of Auckland, Auckland 1142, New Zealand
[3]Commonwealth Scientific and Industrial Research Organisation (CSIRO) Energy, Perth, Western Australia 6151, Australia
[4]Geological Sciences, University of Canterbury, Christchurch 8140, New Zealand

ABSTRACT

Volcano seismicity is an important tool used to monitor volcanic hazards, as seismic signals are commonly associated with fracturing and the movement of volcanic fluids. In investigating the relation between fluids and seismic signals, we record acoustic emissions (AEs) in the laboratory that result from fracturing and fluid depressurization through the fractured rock. We vary the fluid viscosity to create field analogues of hydrothermal and magmatic fluids. While fracturing causes high-frequency volcano-tectonic (VT)–type AE signals, fluid venting results in VT and long-period AEs with variable but overall lower dominant frequencies. The viscosity of the vented fluid correlates (1) inversely with the peak dominant frequency, (2) inversely with the number of induced AEs, (3) proportionally to the onset time of AEs, and (4) inversely with the initial rate of AE generation. Tremor was observed only in the early stages of low-viscosity fluid venting and thus may be more associated with gases and hydrothermal fluids than with magma.

INTRODUCTION

Volcanic seismicity is driven by pressurized or buoyant magmatic and hydrothermal fluids. As such, seismic signals can act as warnings for hazards, such as eruption and dome collapse (Chardot et al., 2015; Miller et al., 1998). Characteristic waveform attributes (e.g., frequency content) of volcano seismic signals can be used to identify distinct geological processes such as faulting or fluid migration.

Volcano-tectonic (VT) seismicity, dominated by relatively high-frequency signal (5–15 Hz), results from brittle failure, triggered as fluids exert stresses on the rock mass (Chouet and Matoza, 2013). Long-period (LP) or low-frequency (LF) signals, with frequencies in the range 0.2–5 Hz and more emergent P-wave onsets (Neuberg et al., 2000), are predominantly ascribed to resonance in fluid-filled cracks and conduits and associated with fluid transport. Hybrid events feature an impulsive VT onset, followed by LP coda (Miller et al., 1998). Finally, volcanic tremor is a long-duration, continuous, and sometimes harmonic signal in a well-defined narrow-band frequency spectrum. It sometimes follows LP events, suggesting a common source mechanism (Neuberg et al., 2000). The analysis of LP-type events is used to infer fluid properties, conduit geometry, and pressurization of a volcanic system, which are important factors in understanding and mitigating risk (Jousset et al., 2013; Saccorotti et al., 2007).

Although fluid mobility is vital for induction of precursory seismicity, we lack knowledge of how fluid viscosity—a key control on flow rate—affects volcano seismicity. Because fluid viscosity is a major influence on eruption style (Gonnermann and Manga, 2007), understanding its relationship to volcano seismicity is of great interest for hazard assessment.

Scaled laboratory experiments may be useful for modeling volcano-seismic processes, as they allow isolation of specific processes under controllable, in situ conditions. Previous experiments have proved successful in using a fluid pressure pulse through a rock fracture to generate acoustic emissions (AEs) analogous to LP, hybrid, and tremor seismicity (Benson et al., 2008, 2014; Fazio et al., 2017). Benson et al. (2014) showed that the dominant frequency of LP events in fractured basalt varied when a pressure pulse of high-temperature water transitioned from liquid to gas phase. Despite these successes, the range of fluid viscosities used to experimentally investigate volcano seismicity has been limited. Here, we explore this relationship by analyzing the temporal, spatial, and spectral characteristics of AE waveforms. AEs are first induced via rock fracture, and subsequently by depressurization of fluids with viscosities representative of realistic volcanic fluids through the resultant damage zone.

METHODS

A 74.5-mm-long, 38-mm-diameter cylindrical core sample of imporous (0.63%) and impermeable (0.6 μD), homogeneous American Black Granite (Pennsylvania, United States) is fractured by applying axial load in a triaxial stress cell. A confining pressure of 1 MPa produces a damage zone of vertical to subvertical intersecting fracture planes, imaged by X-ray computerized tomography (XRCT) (Fig. 1A). Subsequently, the sample is saturated with pressurized fluids of variable viscosity (Table 1). Rapid depressurization of fluid is achieved by venting to the atmosphere via a ball valve connected to the top of the sample. Two sets of depressurization experiments are carried out on this sample, at effective pressure (P_{eff}) conditions of 5 MPa and 20 MPa. A confining pressure of 40 MPa is used for all tests except for the P_{eff} = 5 MPa nitrogen gas experiment (see Fig. DR1 in the GSA Data Repository[1]).

Acoustic emissions for the fracturing and depressurization experiments are recorded on 18 ultrasonic transducers (0.5 MHz peak frequency) embedded in the sample jacket. These transducers are also used as active source-

[1]GSA Data Repository item 2019184, note on magma viscosity and rheology in relation to the depressurization experiments, Figures DR1–DR6, and Video DR1, is available online at http://www.geosociety.org/datarepository/2019/, or on request from editing@geosociety.org.

CITATION: Clarke, J., et al., 2019, The relation between viscosity and acoustic emissions as a laboratory analogue for volcano seismicity: Geology, https://doi.org/10.1130/G45446.1

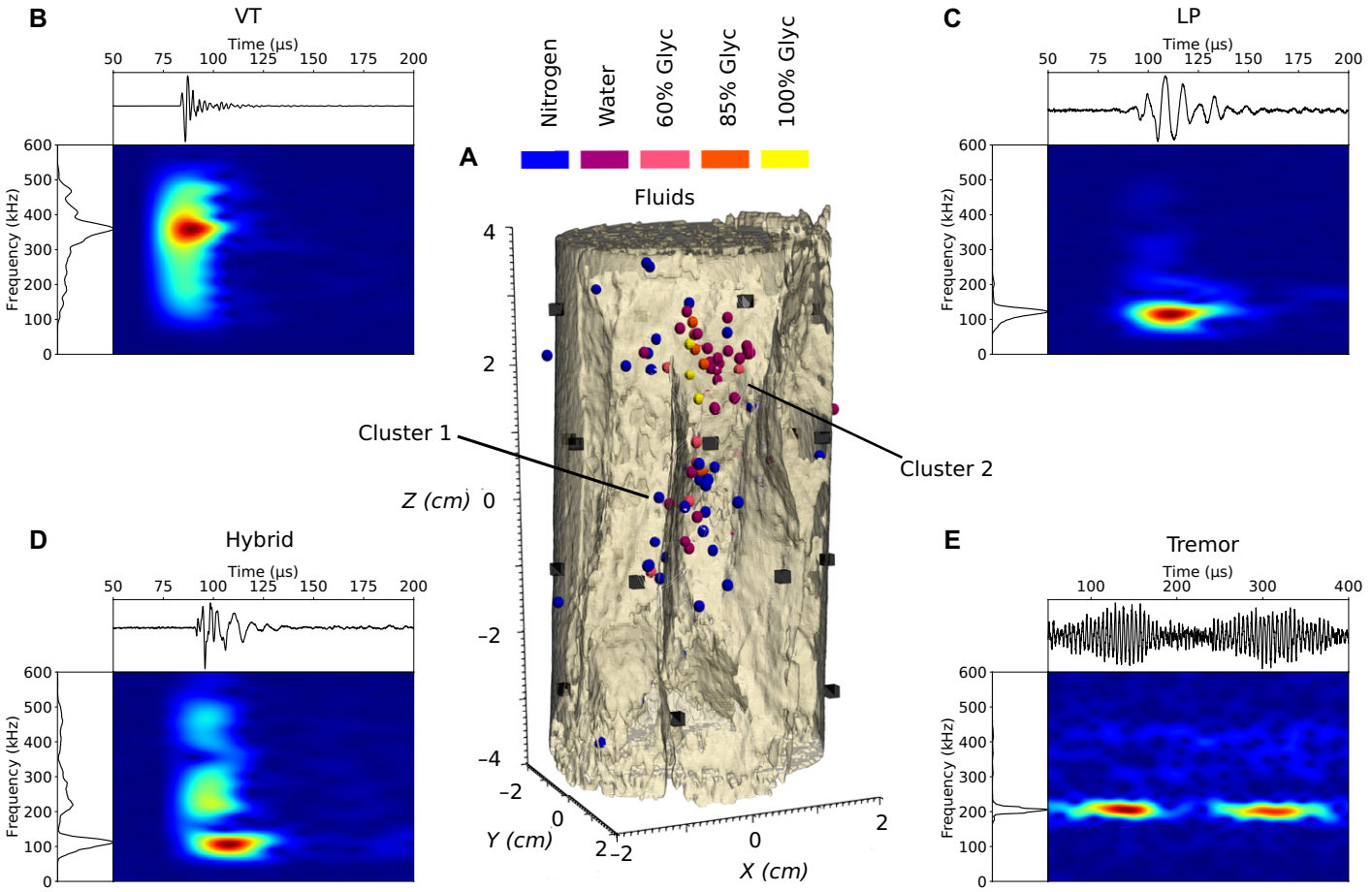

Figure 1. A: X-ray computerized tomography rendering of sample's induced fracture network (sample is American Black Granite from Pennsylvania, United States). Superposed are acoustic emission (AE) locations for both sets of depressurization experiments, color-coded by fluid type that induced event (Glyc—glycerol). Ultrasonic sensor locations are represented by black cubes. Two spatial event clusters are identified. Cluster 1 consists of 21 AEs, which align with 6-cm-long fracture; 52% of these are induced by nitrogen, 24% by water, and 24% by glycerol solutions. Cluster 2 comprises 30 AEs, located toward top of central fracture that runs full length of sample; of these, 7% are induced by nitrogen, 60% by water, and 33% by glycerol solutions. B–E: Representative seismic waveforms for four event types with their normalized spectrogram and power spectrum. For normalized spectrogram intensities, blue represents 0 and red represents 1. B: Volcano-tectonic (VT)–type waveform with impulsive onset and ~350 kHz peak frequency. C: Long period (LP)–type waveform with emergent onset and well-defined low peak frequency, showing little to no energy at high frequencies. D: Hybrid-type waveform, showing impulsive VT onset followed by LP coda. Note "hockey stick" shape of spectrogram. E: Two pulses of continuous tremor-type signal (Fig. DR5 [see footnote 1]) with narrow-band, low-frequency (~200 kHz) spectrogram.

receiver pairs to estimate the rock velocity model for AE location. An event is detected when at least four transducers are triggered by a minimum amplitude of 7 mV within a time window of 100 μs. Spectral information of each AE is gathered from the highest-amplitude waveform, typically recorded on the transducer closest to the source.

Laboratory fluid viscosity is scaled to volcanic analogues by considering an idealized model of parallel plates (Sarkar et al., 2004). The laminar volumetric flow rate Q for a fluid with viscosity μ through a smooth-sided, rigid, and impermeable fracture of length L, width W, and aperture d, under a pressure gradient ΔP, is:

$$Q = \frac{Wd^3\Delta P}{12\mu L}. \quad (1)$$

If Q and ΔP are equal for laboratory and field fluids, then field and laboratory fluid viscosity relate as:

$$\mu_f = \frac{\mu_l L_l W_f d_f^3}{W_l d_l^3 L_f}, \quad (2)$$

where the subscripts l and f represent the laboratory and field, respectively. L_l, W_l and d_l are estimated from the XRCT images to have maximum values of 7.5 cm, 3.8 cm, and 0.6 mm, respectively. We consider field volcanic conduits with a realistic length L_f of ~500 m, a L_f/W_f of ~0.5 and an aspect ratio L_f/d_f of ~10^4, consistent with previous modeling of LP resonance (Kumagai and Chouet, 2001). The μ_f values (Table 1) should be regarded qualitatively, as estimates are sensitive to fracture geometry. In addition, magma has a complex strain-dependent rheology, where fractional crystallization and volatile volumes alter its viscosity (Mader et al., 2013; see the Data Repository). Our experimental fluids are homogeneous and single phase, and thus do not model rheological effects

TABLE 1. VISCOSITY OF LABORATORY FLUIDS AND CALCULATED FIELD EQUIVALENTS

Fluid	Laboratory fluid viscosity, μ_l (Pa·s)	Field equivalent viscosity, μ_f (Pa·s)	Field analogue
Nitrogen	2×10^{-5}	N.A.	Gas
Water	0.001	600	Basaltic magma
60% glycerol	0.01	6000	Andesitic magma
85% glycerol	0.1	6×104	Andesitic magma
100% glycerol	1.4	8×105	Andesitic magma

Note: Laboratory fluid viscosities are from Segur and Oberstar (1951). N.A.—not applicable.

of magmatic flow. Gas flow cannot be modeled by Equation 1, but nitrogen gas represents a realistic analogue for volcanic volatiles.

RESULTS

Cumulative Fluid-Induced Events

We record 249 fluid-induced events for the two P_{eff} conditions. Of these, 66% are induced by venting nitrogen, 25% by water, and 9% by glycerol solutions. For both sets of experiments, the cumulative number of AEs detected in 1 hr following fluid depressurization is inversely proportional to fluid viscosity (Fig. 2; Figs. DR2 and DR3). The initial rate of induced events is essentially equivalent for nitrogen and water but is otherwise inversely proportional to fluid viscosity. The seismic response to fluid depressurization is not instantaneous, and the lag time is proportional to fluid viscosity. For viscous fluids, induced seismicity occurs several minutes after depressurization. For our experiments, number of events n and lag time t_0 follow power laws with respect to viscosity:

$$n = 34.7\mu^{0.3}, \quad (3)$$

and

$$t_0 = 1.5\ \mu^{0.7}. \quad (4)$$

Fluid-Induced Event Locations

An event is located if the P-wave arrival time can be identified on eight or more transducers. Homogeneous velocity models for hypocenter inversion are estimated from active ultrasonic surveys. Event locations generally correlate with the fractures identified in the XRCT images. Two main spatial clusters locate on two orthogonally intersecting fracture planes (Fig. 1; Video DR1). Cluster 2 is associated with a complex intersection of fractures of different scales (Fig. DR4). The least viscous nitrogen-induced events are distributed widely throughout the fractured sample, while events related to venting the more viscous fluids are more localized.

Seismic Signatures

During rock fracturing, 187 AEs are generated with predominantly high frequencies (350 kHz) and impulsive onsets (Fig. 1B), resembling classic VT-type events. Fluid depressurization induces a wider range of event types in terms of frequency content. VT-type events are again present, while AEs featuring an impulsive, high-frequency onset and LF coda (Fig. 1D) are numerous and resemble hybrid seismicity. Low-frequency (<250 kHz) AEs with emergent onsets (Fig. 1C) are less common.

Long-duration signals occur during the initial second(s) of nitrogen venting and exhibit well-defined peak frequencies of ~200 kHz and beating waveforms (Fig. 1E; Fig. DR5) resembling volcanic tremor. These signals are detected in recordings of triggered, individual high-amplitude events, and therefore, the source of the tremor cannot be located as the onset is not recorded. Two LP AEs are identified in periods immediately preceding and during tremor. Comparison of the frequency spectra of these two events with that from tremor show that although they have similar dominant frequencies, the LPs have significantly broader power spectra, suggesting a different source (Fig. DR6).

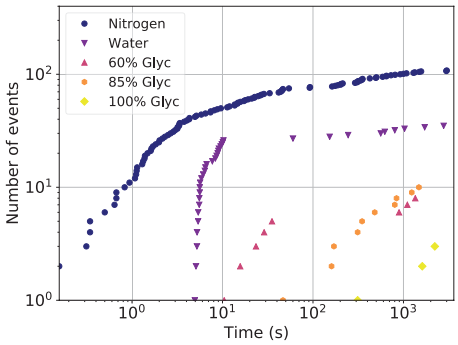

Figure 2. Cumulative number of acoustic emissions induced by fluid type for effective pressure P_{eff} = 5 MPa in 1 hr after fluid pressure release. Glyc—glycerol.

Frequency Analysis

Dominant frequencies are extracted from power spectra for fracturing- and depressurization-generated events. Histograms and kernel density estimates (KDEs; Bors and Nasios, 2009) for AEs generated during fracturing and venting of nitrogen and water are shown in Figures 3A–3C. Events with dominant frequencies of 350 kHz are heavily favored during rock fracture but are also prevalent during venting of all fluids. The dominant frequencies for fluid-induced events have a significantly broader distribution, with a higher contribution from low frequencies, than is seen for AEs associated with rock fracture.

Water-induced events show a distinct bimodal distribution of dominant frequencies, with a low-frequency mode at 126 kHz which may be due to fluid resonance. Such a bimodal distribution is not observed for other fluids. Although tremor-, LP-, and hybrid-type signals are observed during nitrogen venting, no distinct low-frequency mode(s) are seen in the dominant-frequency KDE. It could be that nitrogen venting induces AEs across fractures (resonators) with variable geometries, resulting in resonant waveforms that are not defined by any particular frequency. In contrast, water-induced events are more localized to specific fractures. The recording of relatively few AEs induced by glycerol-based solutions limits our ability to draw statistically robust conclusions on dominant-frequency distributions. The low number of events for such fluids could be due to a lower fluid flow rate associated with higher

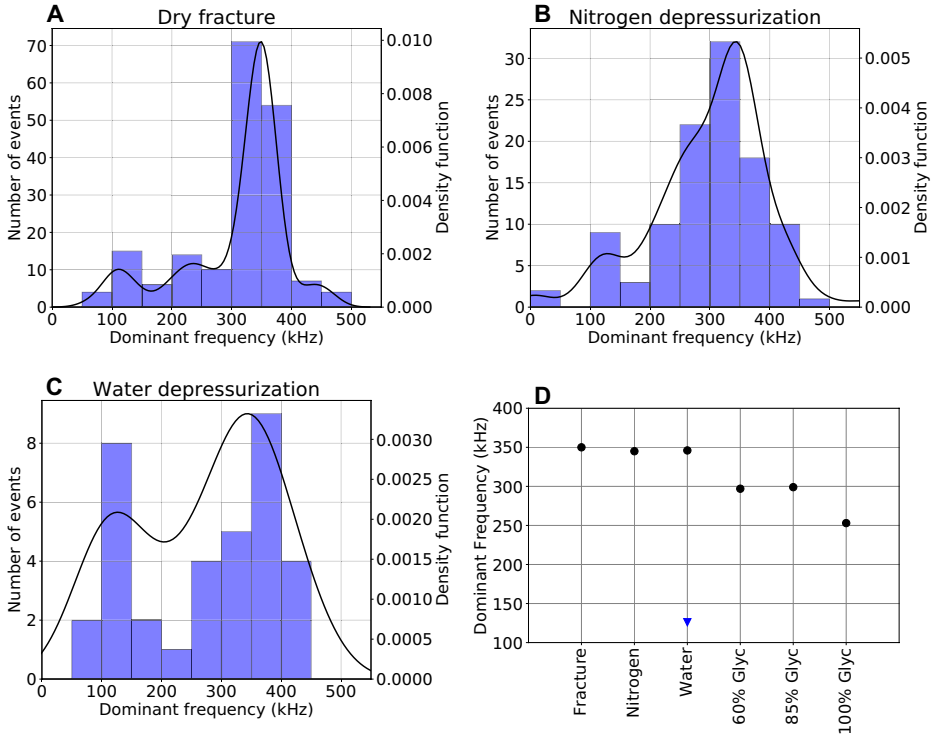

Figure 3. A–C: Histograms and kernel density estimates (KDEs) of dominant frequencies of acoustic emissions recorded during rock fracture (A), depressurization of nitrogen (B), and depressurization of water (C) for effective pressure P_{eff} = 5 MPa. D: Dominant frequency of fracturing and depressurization events (black circles). Depressurization of water induces events with secondary peak in kernel density estimates (KDEs) (blue triangle). Glyc—glycerol.

viscosities inhibiting triggering of AEs, while wave attenuation may limit detection.

The frequency of the maximum of the KDE (Fig. 3D) correlates with fluid viscosity, ranging from ~350 kHz for events generated by nitrogen and water venting to ~250 kHz for events related to venting 100% glycerol. The decrease in frequency content with fluid viscosity is likely primarily due to attenuation that results from (viscous) fluid flow. The fact that high frequencies dominate these spectra suggests that fluid-induced events are also partly associated with fracture mechanics (Benson et al., 2010).

Source Mechanisms

Source mechanisms for 12 events generated by rock fracture and water depressurization are presented on a Hudson *T*-*k* plot (Sarout et al., 2017) in Figure 4. Focal mechanisms are described in terms of constant-volume deviatoric (*T*) and volumetric (*k*) components of deformation. Fracture-induced events cluster around the origin, which represents the pure double-couple source of shear failure. The source mechanisms of water-induced events display a greater spread in the *T*-*k* plot, having significant compensated linear vector dipole (Julian et al., 1998) and volumetric components, indicating that multiple source mechanisms could be at play.

IMPLICATIONS

Volcanology stands to benefit from a deeper understanding of the role of (viscous) fluids in volcano seismicity. To interpret our experimental AEs in the context of volcano seismicity, we apply a commonly used, linear frequency-dimension scaling relationship (Benson et al., 2008):

$$L_l \times F_l = L_f \times F_f. \quad (5)$$

For our laboratory sample with fracture length L_l = 7.5 cm and typical LP waveform frequency $F_l \approx$ 100 kHz, the equivalent field frequency F_f = 7.5 Hz for field conduits of length L_f = 1 km. LP events in the field are typically <5 Hz (Neuberg et al., 2000).

From our experiment, we hypothesize that a tremor-like signal is generated preferentially by fast-moving gas. This compares favorably to interpretations of tremor at Ruapehu volcano (North Island, New Zealand), where Hurst and Sherburn (1993) suggested resonant excitation by the "white noise" signal of high-pressure gas flow to be a possible mechanism. Field observations of discreet LP events merging into continuous tremor (Neuberg et al., 2000) suggest that tremor may be a superposition of LP events. Although we do record discrete LP events with a similar peak frequency coincident with tremor, LPs show a markedly broader power spectrum, which as pointed out by Hurst and Sherburn (1993) is inconsistent with the superposition hypothesis.

The glycerol mixtures generated relatively few AEs, suggesting that the contribution of migrating high-viscosity magmas to the overall seismicity at active volcanoes may be small compared to low-viscosity fluids such as brines and gas. The presence of LP- and hybrid-type glycerol-induced events supports the idea that viscous magma melt migration contributes to LP seismicity (Burlini et al., 2007).

The peak dominant frequency of induced AEs appears to decrease with fluid viscosity. Field seismic observations have related decreasing spectral content of LP events to increasing gas volume in two-phase mixtures, explained by resonating and scattering mechanisms (Jolly et al., 2012). Our data suggest that variations in fluid viscosity may offer a complementary explanation for such frequency shifts in volcano seismic signals.

Wave attenuation due to viscoelasticity and scattering appears to have a significant effect on the frequency spectra of detected experimental events. This is also true in volcanic settings and may be compounded when seismometers are far from the source (Bean et al., 2014). It has been suggested that slow fracture rupture in unconsolidated material represents an alternative source mechanism for LP seismicity (Bean et al., 2014). The role of path and source effects is a critical point to pursue in further work to truly understand VT and LP signals in the laboratory and field.

Our experiments provide insight into how volcano seismicity relates to the movement of pressurized fluids through rock fractures—a process thought to be key to generation of LP seismicity. Our results suggest that the viscosity of volcanic fluids may have an effect not only on the frequency spectra of seismicity but also on the number of events, lag time, rate, and spatial distribution.

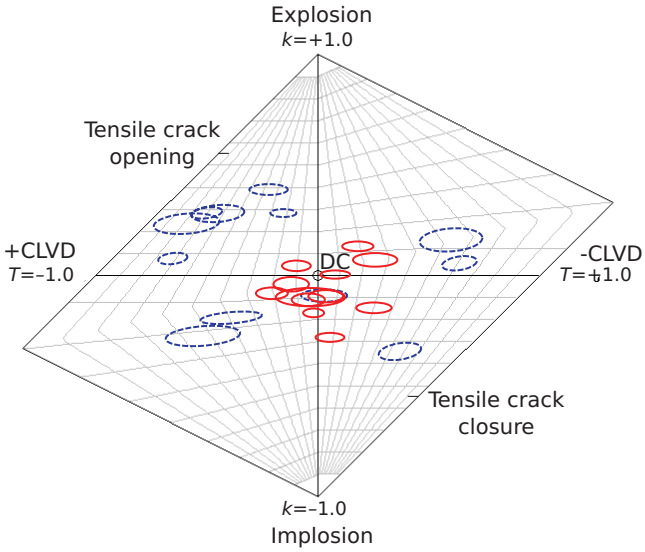

Figure 4. Hudson *T*-*k* plot (*T*, deviatoric component; *k*, volumetric component) showing error ellipses of source mechanism for 12 events generated during fracturing (red, solid) and water depressurization (blue, dashed). Only selected events where P-wave polarity can be picked with confidence on eight or more transducers are inverted for source mechanisms. DC—double couple; CVLD—compensated linear vector dipole.

ACKNOWLEDGMENTS

This research is funded by New Zealand Earthquake Commission grant 14/U690. Kennedy thanks the New Zealand Natural Hazards Research Platform for funding. We thank CSIRO Energy for the Geomechanics and Geophysics Laboratory facilities, and L. Esteban and S. Kager. We thank P. Benson and two anonymous reviewers for constructive feedback.

REFERENCES CITED

Bean, C.J., De Barros, L., Lokmer, I., Métaxian, J.-P., O'Brien, G., and Murphy, S., 2014, Long-period seismicity in the shallow volcanic edifice formed from slow-rupture earthquakes: Nature Geoscience, v. 7, p. 71–75, https://doi.org/10.1038/ngeo2027.

Benson, P.M., Vinciguerra, S., Meredith, P.G., and Young, R.P., 2008, Laboratory simulation of volcano seismicity: Science, v. 322, p. 249–252, https://doi.org/10.1126/science.1161927.

Benson, P.M., Vinciguerra, S., Meredith, P.G., and Young, R.P., 2010, Spatio-temporal evolution of volcano seismicity: A laboratory study: Earth and Planetary Science Letters, v. 297, p. 315–323, https://doi.org/10.1016/j.epsl.2010.06.033.

Benson, P.M., Vinciguerra, S., Nasseri, M.H.B., and Young, R.P., 2014, Laboratory simulations of fluid/gas induced micro-earthquakes: Application to volcano seismology: Frontiers of Earth Science, v. 2, 32, https://doi.org/10.3389/feart.2014.00032.

Bors, A.G., and Nasios, N., 2009, Kernel bandwidth estimation for nonparametric modeling: IEEE Transactions on Systems, Man, and Cybernetics: Part B, Cybernetics, v. 39, p. 1543–1555, https://doi.org/10.1109/TSMCB.2009.2020688.

Burlini, L., Vinciguerra, S., Di Toro, G., De Natale, G., Meredith, P., and Burg, J.P., 2007, Seismicity preceding volcanic eruptions: New experimental insights: Geology, v. 35, p. 183–186, https://doi.org/10.1130/G23195A.1.

Chardot, L., Jolly, A.D., Kennedy, B., Fournier, N., and Sherburn, S., 2015, Using volcanic tremor for eruption forecasting at White Island volcano (Whakaari), New Zealand: Journal of Volcanology and Geothermal Research, v. 302, p. 11–23, https://doi.org/10.1016/j.jvolgeores.2015.06.001.

Chouet, B.A., and Matoza, R.S., 2013, A multi-decadal view of seismic methods for detecting precursors of magma movement and eruption: Journal of Volcanology and Geothermal Research, v. 252, p. 108–175, https://doi.org/10.1016/j.jvolgeores.2012.11.013.

Fazio, M., Benson, P.M., and Vinciguerra, S., 2017, On the generation mechanisms of fluid-driven seismic signals related to volcano-tectonics: Geophysical Research Letters, v. 44, p. 734–742, https://doi.org/10.1002/2016GL070919.

Gonnermann, H.M., and Manga, M., 2007, The fluid mechanics inside a volcano: Annual Review of Fluid Mechanics, v. 39, p. 321–356, https://doi.org/10.1146/annurev.fluid.39.050905.110207.

Hurst, A.W., and Sherburn, S., 1993, Volcanic tremor at Ruapehu: Characteristics and implications for the resonant source: New Zealand Journal of Geology and Geophysics, v. 36, p. 475–485, https://doi.org/10.1080/00288306.1993.9514593.

Jolly, A.D., Neuberg, J., Jousset, P., and Sherburn, S., 2012, A new source process for evolving repetitious earthquakes at Ngauruhoe volcano, New Zealand: Journal of Volcanology and Geothermal Research, v. 215, p. 26–39, https://doi.org/10.1016/j.jvolgeores.2011.11.010.

Jousset, P., Budi-Santoso, A., Jolly, A.D., Boichu, M., Surono, Dwiyono, S., Sumarti, S., Hidayati, S., and Thierry, P., 2013, Signs of magma ascent in LP and VLP seismic events and link to degassing: An example from the 2010 explosive eruption at Merapi volcano, Indonesia: Journal of Volcanology and Geothermal Research, v. 261, p. 171–192, https://doi.org/10.1016/j.jvolgeores.2013.03.014.

Julian, B.R., Miller, A.D., and Foulger, G.R., 1998, Non-double-couple earthquakes 1. Theory: Reviews of Geophysics, v. 36, p. 525–549, https://doi.org/10.1029/98RG00716.

Kumagai, H., and Chouet, B.A., 2001, The dependence of acoustic properties of a crack on the resonance mode and geometry: Geophysical Research Letters, v. 28, p. 3325–3328, https://doi.org/10.1029/2001GL013025.

Mader, H.M., Llewellin, E.W., and Mueller, S.P., 2013, The rheology of two-phase magmas: A review and analysis: Journal of Volcanology and Geothermal Research, v. 257, p. 135–158, https://doi.org/10.1016/j.jvolgeores.2013.02.014.

Miller, A.D., Stewart, R.C., White, R.A., Luckett, R., Baptie, B.J., Aspinall, W.P., Latchman, J.L., Lynch, L.L., and Voight, B., 1998, Seismicity associated with dome growth and collapse at Soufriere Hills Volcano, Montserrat: Geophysical Research Letters, v. 25, p. 3401–3404, https://doi.org/10.1029/98GL01778.

Neuberg, J., Luckett, R., Baptie, B., and Olsen, K., 2000, Models of tremor and low-frequency earthquake swarms on Montserrat: Journal of Volcanology and Geothermal Research, v. 101, p. 83–104, https://doi.org/10.1016/S0377-0273(00)00169-4.

Saccorotti, G., Petrosino, S., Bianco, F., Castellano, M., Galluzzo, D., La Rocca, M., Del Pezzo, E., Zaccarelli, L., and Cusano, P., 2007, Seismicity associated with the 2004–2006 renewed ground uplift at Campi Flegrei Caldera, Italy: Physics of the Earth and Planetary Interiors, v. 165, p. 14–24, https://doi.org/10.1016/j.pepi.2007.07.006.

Sarkar, S., Toksoz, M.N., and Burns, D.R., 2004, Fluid flow modeling in fractures: Cambridge, Massachusetts, Massachusetts Institute of Technology, Earth Resources Laboratory Industry Consortia Annual Report 2004-05, 41 p.

Sarout, J., Le Gonidec, Y., Ougier-Simonin, A., Schubnel, A., Guéguen, Y., and Dewhurst, D.N., 2017, Laboratory micro-seismic signature of shear faulting and fault slip in shale: Physics of the Earth and Planetary Interiors, v. 264, p. 47–62, https://doi.org/10.1016/j.pepi.2016.11.005.

Segur, J.B., and Oberstar, H.E., 1951, Viscosity of glycerol and its aqueous solutions: Industrial & Engineering Chemistry, v. 43, p. 2117–2120, https://doi.org/10.1021/ie50501a040.

Printed in USA